Paper

SIMULTANEOUS EXPOSURE USING 532 AND 860 nm LASERS FOR VISIBLE LESION THRESHOLDS IN THE RHESUS RETINA

William Roach,* Robert Thomas,* Gavin Buffington,† Garrett Polhamus,* John Notabartolo,* Cheryl DiCarlo,‡ Kevin Stockton,§ David Stolarski,§ Kurt Schuster,§ Val Carothers,§ Benjamin Rockwell,* and Clarence Cain§

Abstract—The growth of commercially available, simultaneous multi-wavelength laser systems has increased the likelihood of possible ocular hazard. For example, many systems utilize frequency multiplying methods to produce combinations of visible, near-infrared, and ultraviolet wavelengths. Unfortunately, very little data exists to substantiate the current methods for estimating hazards from simultaneous lasing. To properly assess the retinal hazards from these wavelengths, the retinal effects of 10-s laser irradiation from 532 and 860 nm were determined in non-human primates for four different relative dosage combinations of these wavelengths. This pair of wavelengths represents the typical problem of a visible-wavelength laser combined with an in-band, infrared wavelength that is not as well focused at the retina—a situation difficult to address. To add confidence to the experimental results obtained, a theoretical thermodynamic model was developed to predict the minimal damage threshold for simultaneous wavelengths at 1 h post exposure. The new model calculations and the data obtained are compared with results from one currently accepted method of predicting relative exposure limits from multi-wavelength systems. In addition, the current ANSI-Z136-2000 standard was used to compute the combined MPEs for comparison with measured visible lesion thresholds. A total of 12 eyes were exposed using four different ratios of power levels (532/860 power rations) to determine the contribution to the damage levels from each wavelength. The experimental data were analyzed using probit analysis at both 1-h and 24-h post exposure to determine the minimum-visible-lesion (MVL) thresholds at ED_{50} values, and these thresholds at 24 h varied from 5.6 mW to 17 mW total intraocular power.

Health Phys. 90(3):241–249; 2006

Key words: analysis, statistical; laboratory animals; lasers; maximum permissible exposures

* U.S. Air Force Research Laboratory, Optical Radiation Branch, Brooks AFB, TX 78235-5278; † Fort Hays State University, Department of Physics, Hays, KS 67601; ‡ U.S. Army Medical Research Detachment, Walter Reed Army Institute of Research, Brooks AFB, TX 78235-5278; § Northrop Grumman, 4241 Woodcock Drive, Suite B-100, San Antonio, TX 78228-1330.

For correspondence or reprints contact: W. Roach, U.S. Air Force Research Laboratory, Optical Radiation Branch, Brooks AFB, TX 78235-5278, or email at william.roach@brooks.af.mil.

(*Manuscript received* 3 *May* 2005; *revised manuscript received* 25 *July* 2005, *accepted* 22 *October* 2005)

0017-9078/06/0

INTRODUCTION

THE GOAL of this study was to investigate the potential for synergistic effects of simultaneous laser exposures and to determine the minimum visible lesion (MVL) thresholds for different ratios of powers from two lasers of different wavelengths operating simultaneously. The increase of lasers or laser systems operating with multiple wavelengths simultaneously is on the rise in commercial, research, and military settings. According to the American National Standards Institute (ANSI) Standard for Safe Use of Lasers (ANSI 2000), the maximum permissible exposure (MPE) values are below known tissue damage levels but may be uncomfortable to view or feel on the skin, though they are considered unable to cause permanent biological damage. This standard states that it is good practice to maintain exposure levels sufficiently below the MPE to also avoid discomfort. Distractions from the laser beam, such as flash blindness, glare, and startle, which can create secondary hazards, have become an increasing concern.

Two widely separated wavelengths, 532 nm and 860 nm, were used for simultaneous lasing in our experimental setup in order to simulate an ongoing vision science experiment for purposeful lasing. Caution was required in deriving the combined wavelength MPEs for these exposure situations, and the calculations for the MPEs as outlined in the ANSI standard are complex. In general, for multi-wavelength exposure occurring simultaneously, the standard states that the effects of such exposures from pulsed- and continuous wave (CW)-laser radiation may act synergistically. For multiple wavelength laser emissions, the MPE must first be determined for each wavelength separately. Exposures from several wavelengths in the same time domain are additive on a proportional basis of spectral effectiveness with due allowance for all correction factors. Also, in our particular application to the safety of purposeful viewing, the maximum required exposure duration was 10 s. Therefore, the common aversion response time (0.25 s) to visible light was not

allowable when performing the safety analysis. Thus, 10-s exposure durations were used in this particular damage threshold experiment.

METHODS

Experimental laser setup

Fig. 1 shows that the equipment used in our setup starts with a Spectra Physics Millennia X, 10W, 532 nm laser (Available at http://www.spectra-physics.com). The beam was split into two with a 50/50 532-nm beam-splitter. The transmitted part of the beam was then directed into a Spectra Physics Model 2900, Ti:Sapphire laser as the pump source and provided an output tuned to 860 nm. The reflected part of the 532-nm beam was directed through a cube and waveplate combination to vary the power independently without affecting the tuning of the Model 3900 Ti:Sapphire. This beam was then combined with a helium-neon beam (632 nm) for alignment as shown in Fig. 1. The 860-nm beam from the Model 3900 was then combined with a 532/632-nm beam and aligned coaxially through a set of irises. The combined beams were then passed through a Fresnel rhomb prism and polarizing cube to vary the power for both the 532-nm and 860-nm beams simultaneously. The beams were then passed through a limiting aperture and a controlling shutter (not shown) before being directed through the periscope. After the beams were raised to the height of the fundus camera, they were directed past the front lens of the camera to be split again by a 50% silvered mirror. The reflected beam was directed into the subject's eye, and the transmitted portion was directed into a reference detector. The Laser Precision RM6600 power meter and RKP575 detector heads (Laser Probe, Inc., 23 Wells Avenue, Utica, NY 13502) monitored and measured the output power of the reference beam through the 50% silvered mirror.

Four sets of independent measurements of the MVL thresholds were taken. A ratio of 7/1 for the powers generated by the two lasers for 532/860 nm was used in the first set of measurements. In addition to this ratio, three other ratios were used for the measurement of the MVL thresholds: 1/1, 1/3, and 0/1 for the 532/860 power ratio. A ratio of 1/0, or 100% 532-nm exposure, was not conducted as several data points were available in the literature.

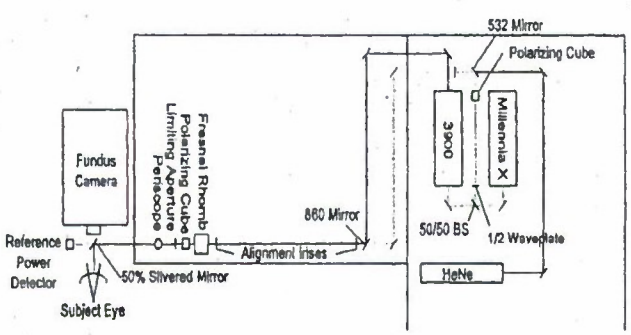

Fig. 1. Schematic layout of laser system used for measurements.

MVL study

Mature *Macaca mulatta* primates from 3 to 8 kg were maintained under standard laboratory conditions (12 h light, 12 h dark). The subjects were screened before exposure to ensure that no eye was more than 0.5 diopter from being emmetropic. Procedures were performed during the light cycle. Animals involved in this study were procured, maintained, and used in accordance with the Federal Animal Welfare Act, the Guide for the Care and Use of Laboratory Animals prepared by the Institute of Laboratory Animal Resources, National Research Council, and the ARVO Resolution for the Use of Animals in Ophthalmic and Vision Research.

Subjects had food withheld for 12 h prior to procedure and were chemically restrained using 10 mg kg^{-1} ketamine hydrochloride (HCl) intramuscularly (IM) injected by veterinary staff. Once restrained, 0.16 mg atropine sulfate was administered subcutaneously. Two drops of proparacaine HCl 0.5%, phenylephrine HCl 2.5%, and tropicamide 1% were each administered to both eyes to allow cycloplegia as well as dilation for fundus photography. Gauze pads were taped over both eyes to protect the eyes and to keep them moistened during transport. Each subject was evaluated immediately after arrival at the laboratory facility for level of anesthesia. Ketamine HCl was re-administered IM as indicated. Under ketamine restraint, the subject's arm hair was clipped, and the area over and surrounding the superficial saphenous veins was cleansed with a betadine scrub and solution followed with an isopropyl alcohol rinse. Twenty-two to twenty-three gauge intravenous catheters were placed and securely taped in each arm for administration of warmed NaCl 0.9% or Lactated Ringers solution (10 mL kg^{-1} h^{-1} flow rate) and for administration of propofol. An initial induction (bolus) dose of propofol (2–10 mg kg^{-1}) was administered to effect.

A state of anesthesia was maintained using 0.2–1.0 mg kg^{-1} min^{-1} of propofol via syringe pump. The subject was intubated with a cuffed endotracheal tube of appropriate size. A peribulbar injection of either 4% lidocaine or cocktail mix of equal amounts of 2% lidocaine/bupivacaine 0.75% (with 0.1 mL hyaluronidase to improve tissue perfusion) was administered with a 25 gauge, 0.5–0.75-inch needle, to minimize extraocular muscular movement during exposure. The subject was securely restrained in a prone position on an adjustable

stage for fundus photography, laser exposure, and fluorescein angiography (FA). The subject's eye was kept open with an ophthalmic speculum, and frequently rinsed with 0.9% saline solution to maintain moisture during the procedure. Approximately 15 min prior to Fluorescite administration, acepromazine (0.5–1.0 mg kg^{-1}) was administered intravenously as an antiemetic. Immediately prior to FA, 0.6 mL of Fluorescite 10% (Alcon Laboratories, http://www.alconlabs.com) was administered as an intravenous bolus followed by a NaCL flush or Lactated Ringers IV push. The subject's heart rate, oxygen saturation, and respiratory rate were continuously monitored throughout the experimental protocol using a pulse oximeter. Normal body temperature was maintained by the use of circulating warm water blankets. After completion of the procedure, the subject was transported back to the prep room where it was monitored for recovery from the anesthetic agents. Upon arousal, the subject was extubated and transported back to the animal housing area.

The retina was viewed with a fundus camera, and exposures were delivered to the macular region within a five-by-five grid. Marker lesions were created with approximately 90-mW, 90-ms, single-pulse exposures at 532 nm to define one margin of the grid rows and columns. These marker lesions allowed precise placement of experimental lesions in a pre-defined grid. Power levels for the 10-s exposures (50 to 100 shots) were varied from approximately one-tenth to 4 times the ED_{50} value, and the number of eyes varied between 2 and 4. The subject was maintained under anesthesia throughout the 1-h post-laser evaluation. At 24 h after laser treatment, the subject was again anesthetized following the protocol but without peribulbar injection. All eyes were evaluated at 1 h and 24 h post-exposure by three experienced readers and visible lesions at a given exposure site were reported as a "yes" only if at least two readers identified a lesion. Color fundus photographs were taken before exposures and after 1 h and 24 h.

Energy delivered, along with a "yes" or "no" value, was recorded if a lesion was or was not observed on the retina at each laser delivery site by each reader. A probit data analysis technique (Finney 1971; Cain and Noojin 1996) was applied to the "yes" or "no" recorded as a one or zero, respectively, for each dosage applied. This analysis provided the estimated dosage to cause a MVL with 50% probability (ED_{50}) and confidence intervals [fiducial limits (FL) at the 95% confidence level].

Modeling of damage thresholds

Experimental determination of the threshold for damage from the combined two-wavelength emitter is documented here. In order to add to the confidence in these results, standard thermodynamic models have been applied to the system. In the case of a 10-s exposure, the damage to the retina from a 532-nm or 860-nm laser is known to be thermal in nature (Welch and Van Gemert 1995). Several works exist in the literature that provide modeling methods as well as a broad range of validating data to the mathematical description of the thermal laser damage to the retina (Mainster et al. 1970a; Takata et al. 1974; Welch and Polhamus 1984; Birngruber et al. 1985; Vogel and Birngruber 1992). This work has been drawn upon and implemented into a more generalized version of the models, which allows for the combination of several source terms and evaluation of the subsequent damage predicted.

The model implemented here numerically computes the solution to the heat conduction equation for a multilayer system. This equation is expressed in cylindrical coordinates by eqn (1):

$$\rho c \frac{\partial v}{\partial t} = \frac{\kappa}{r}\frac{\partial v}{\partial r} + \frac{\partial}{\partial r}\left(\kappa \frac{\partial v}{\partial r}\right) + \frac{\partial}{\partial z}\left(\kappa \frac{\partial v}{\partial z}\right) + A. \tag{1}$$

In eqn (1), $v = v(z, r, t)$ is the temperature rise (in Kelvin) in the tissue as a function of time and position. Several values are required to determine this temperature rise. The value $\kappa = \kappa(z)$ is the thermal conductivity (in J cm^{-1} s^{-1} K^{-1}), $c = c(z)$ is the specific heat (in J g^{-1} K^{-1}), and $\rho = \rho(z)$ is the density (in g cm^{-3}). The function $A = A(z, r, t)$ is the source term (in J cm^{-3} s^{-1}), representing energy absorbed per unit time and volume.

For the problem of heat deposition and time dependence of eqn (1), the source term is determined by the properties of the laser beam as well as the optical and thermal properties of the tissue. In this model, the source term has been generalized to allow for the combination of a wide variety of sources with cylindrical symmetry:

$$A(z, r, t) = \sum_{k=1}^{N} \int_{\lambda_1}^{\lambda_2} h_k(z, r, t) H_{0k}(\lambda, t) \beta(z, \lambda) \exp[-\beta(z, \lambda)\delta z] d\lambda. \tag{2}$$

This source term provides a time-dependent description of the linear absorption of optical energy as a function of depth in the tissue, complete with spectral and radial dependence of energy being absorbed. In eqn (2), the indexed values of k refer to independent sources incident on the tissue. The value λ represents the wavelength (in nm), $h_k(z, r, t)$ is the spatial and temporal irradiance profile of the optical source in cylindrical coordinates

(unitless), $H_0(\lambda, t)$ is the irradiance of the optical source as a function of wavelength and time, and $\beta(z, \lambda)$ represents the absorption coefficient at a given position within the tissue. The δz_j above represents a single axial grid point spacing. The generalized source term in eqn (2) provides the ability to combine any number of laser or broadband sources absorbed by any number of tissue types each with differing absorption properties.

The model implements a finite-difference solution to the time-dependent partial differential equation in eqn (1). An alternating-direction implicit solution has been applied as documented in the literature by Peaceman and Rachford (1955) and Mainster et al. (1970b). We have performed validation of the model against the results presented in Mainster et al. (1970b) and the comprehensive work by Welch et al. (1978).

Within the current model, the source may include one or many single wavelength laser sources. For broadband sources, the spectrum may be specified as an input, or a blackbody distribution corresponding to a known color temperature can be computed. Spatial profiles may be Gaussian, flat-top, annular, or user-defined. Temporal profiles may be single or multiple square pulses, or the temporal behavior may be user-defined for each time point. In all cases, the model determines an adaptive time step, which captures rapid changes in temperature at high time resolution. The adaptive time step also provides for large time steps in regions for which there is little change in the temperature distribution (steady state). Finally, the grid point spacing is defined by the user along with the minimum and maximum coordinates for the grid. A "stretched-grid" formalism is also included to add exponentially increasing grid point spacing outside of the regions of most interest (i.e., away from the optical radiation exposure area). This stretched grid allows for maximum computation speed, while minimizing the effects of the imposed boundary condition of no temperature rise at the large radial coordinates and at axial coordinal maximum and minimum boundaries.

The temperature-rise time-history solution to our problem, $\nu(z, r, t)$, is captured and processed through the application of an Arrhenius reaction rate equation, which takes the form:

$$\Omega(z, r) = C\int_{t_1}^{t_2} \exp\left(\frac{-E}{RT}\right)dt, \qquad (3)$$

where C is a pre-exponential normalization constant (s^{-1}) from experimental work (Welch and Van Gemert 1995), E represents the activation energy for the reaction (cal M^{-1}), R is the universal gas constant (2.0 cal M^{-1} K), $T = T(z, r, t)$ is the absolute temperature at position and time (K), and $\Omega(r, z)$ is commonly referred to as a criterion for damage. The values of t_1, and t_2 represent initial and final times of computations contained during a given simulation.

Several works have experimentally determined the values of C and E in eqn (3). (Takata et al. 1974, 1977; Welch et al. 1978; Birngruber et al. 1983; Welch and Polhamus 1984; Birngruber et al. 1985). Welch and Polhamus (1984) experimentally determined for the retina that $C = 1.3 \times 10^{99}$ s^{-1}, and $E = 1.5 \times 10^5$ cal M^{-1}. These values represent thresholds for damage evaluated at 1-h post exposures. Other values exist in the literature and are based upon differing assumptions about tissue types and geometry. Because of this, tissue geometry consistent with the model documented by Welch and Polhamus was selected. Our model therefore provides self-consistent results that can be compared to previous modeling studies that were experimentally validated. The simple tissue geometry selected is illustrated in Fig. 2. Layer thickness values for both the vitreous and sclera represent essentially "infinite" thickness, providing a solution for axial boundaries at which very little energy is conducted within an 11-s simulation time. They are not intended to represent an exact physiological construct. The maximum radial extent of approximately five millimeters provides the same "infinite" extent. Optical and physical parameters relevant to the solution of eqn (1) and definition of the source term with eqn (2) are provided in Table 1 and Table 2.

Absorption coefficients for the retinal pigment epithelial (RPE) layer as a function of wavelength are important parameters within this thermal model. A value of 1,428 cm^{-1} is provided by the previously validated model case of 514.5 nm, but that validation does not include exposures at a wavelength of 860 nm. This study

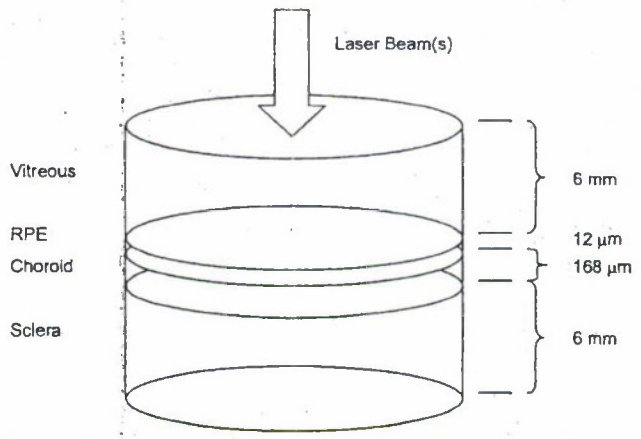

Fig. 2. Tissue layers and geometry employed in the thermal model estimates of damage thresholds.

Table 1. Tissue parameters employed in the thermal model estimates of damage thresholds.

Parameter	Vitreous	RPE	Choroid	Sclera	Units
Thickness	6,000	12	168	6,000	μm
Thermal conductivity	6.28×10^{-3}	6.28×10^{-3}	6.28×10^{-3}	6.28×10^{-3}	J s^{-1} cm^{-1} K^{-1}
Specific heat	4.19	4.19	4.19	4.19	J g^{-1} K^{-1}
Density	1.0	1.0	1.0	1.0	g cm^{-3}
Absorption coefficient (at 532 nm)	0.0	1,485	166	166	cm^{-1}
Absorption coefficient (at 860 nm)	0.0	140	10	10	cm^{-1}

Table 2. Laser beam parameters employed in the thermal model estimates of damage thresholds.

Parameter	Beam 1	Beam 2	Units
Wavelength	532	860	nm
Beam diameter at RPE	30	60	μm
Transmittance of ocular media to anterior RPE	75	85	%
Exposure duration	10	10	s
Total simulation time	11	11	s

used the absorption coefficient trend provided by Mainster et al. (1970b) for the retina to estimate a value for use in the thermal model. This trend yields a value of approximately 140 cm^{-1} at 860 nm, which is perhaps our largest source of uncertainty. For example, comparative data from the literature includes the work of Vogel and Birngruber (1992), which utilized an RPE layer thickness of 10 microns with absorption coefficients of 1,506 cm^{-1} and 146 cm^{-1} at 532 nm and 810 nm, respectively, for human RPE. Exercising our model with these particular parameters yields a good agreement predicted damage threshold (less than 10% at 514 nm and approximately 50% difference in the infrared for 810 nm) for our model. Additional uncertain parameters include the reflectance at layer interfaces and the transmittance through the ocular media anterior to the retina. Estimates of these values were obtained from the compiled data of Takata et al. (1974) and the works of Boettner (1967) and Maher (1978). Values for the calculations at specific wavelengths of 532 and 860 nm are included in Tables 1 and 2.

Thermal damage models of the type described in the literature (Mainster et al. 1970b; Takata et al. 1974; Welch and Polhamus 1984; Birngruber et al. 1985; Vogel and Birngruber 1992) incorporate a numerical simulation of thermodynamics coupled with a single term rate process model and have demonstrated that very small image size (less than 100 μm) estimates of damage thresholds for 10-s exposures are often inaccurate from the perspective of lesion detection limits. Often, for a Gaussian beam profile the thermal model will indicate damage of a scale equal to a single grid point in the simulation, a dimension less than the size of a single cell in the retinal pigment epiththelia. Also, there is considerable discrepancy between experimental measurements and model predictions for the maximum temperature achieved in the central region of the source. The MVL diameter at threshold has been determined to be about 80 μm in the case of a 514.5-nm, 10-s, small image size source as reported by Welch and Polhamus (1984). Combining past model and experimental results has led to the conclusion that for a long exposure time, up to 10 s, the MVL lesion size on the retina is typically limited to about 60–80 μm in diameter at detection threshold (Thomas et al. 2001). This has been attributed to scattering effects, thermal lensing within the eye, or variations in effective ocular accommodation at the retinal pigment epithelial layer (Welch and Polhamus 1984).

Due to these model restrictions for the small image sizes, a more consistent method of estimating the damage threshold was applied. The formation of a lesion (40-μm in radius) was selected as a criterion for damage, which is consistent with experimental measurements. This provides a threshold criterion which is less sensitive to source size for small beam diameter values, and constitutes a validated threshold lesion size for a 10-s exposure (Welch et al. 1978; Welch and Polhamus 1984).

Although very flexible in terms of assigning source terms to irradiate tissue and observe the resulting damage, the model is limited in several regards and relies on some fundamental assumptions that limit applicability. Currently, the model does not support phase changes in the medium. It assumes that temperature rise near threshold for damage is less than the boiling point of the tissue, which in fact may lead to an underestimate of the temperature rise required for damage as shown by Neumann and Brinkmann (2005) for micro- and nanosecond laser pulse exposure on porcine retinal pigment epithelial melanosomes. All responses are assumed to be linear with little change in density or thermodynamic

properties as a function of temperature. Perfusion effects have also been neglected for the purposes of the validation studies here, as it has been shown that they are not significant for the simulation durations of less than 10 s presented here. Optical propagation within the model is rudimentary. Although a hyperbolic description of the focal geometry can be specified as a function of time, effects of scattering are ignored as well as any nonlinear propagation effects. In this study where we have broadband sources, we have ignored chromatic aberrations of the eye which would be manifested for very small image diameters at the furthest infrared and ultraviolet wavelengths studied. Finally, photochemical damage mechanisms are not considered for this work.

RESULTS

MVL study

Results of the MVL threshold measurements are given in Table 3 for both the 1-h reading and the 24-h post-exposure reading together with their FL calculated at the 95% confidence level. Also, the slope of the probit curve at the 50% probability for the 24-h reading is shown in the last column for each power ratio. In all four trials, the thresholds at 24 h were lower than the value at 1 h. The FL calculated for all ED_{50} thresholds at both the 1-h and 24-h times were within 50% of the ED_{50} value with the exception of the upper FL for the 1/3 ratio at 24 h. However, only two eyes were exposed at this ratio using 50 exposures because the slope was extremely large and the probability of Chi-square distribution was 1.00. Since the actual Chi-square test is a measure of how well the predicted distribution fits the experimental data, a probability of 1.00 indicated that the fit was satisfactory. Thus it was not necessary to take additional data points. All powers calculated in Table 3 are the total intraocular powers entering the eye for a 2.5-mm-diameter beam for both co-axial wavelengths. In order to compare these values with the MPEs for the eye, they must be converted to irradiances at the cornea using a 7-mm diameter pupil size.

Modeling results

The results that were obtained from the model are illustrated in Table 4 and in Fig. 3. The model was applied to the experimentally measured ratios of 532-nm and 860-nm exposures. Thresholds were also computed at intermediate values of exposure ratios in order to improve the detail in the trend curves. The thresholds predicted provide a good agreement with the experimental data. The comparison to 1-h damage thresholds agree to within the 95% confidence interval determined through the probit analysis procedure, with the exception of the 75% 860-nm content, for which the value is within about 0.5 mW. This data set was for the 532/860 nm power ratio of 1/3 and utilized only two eyes as listed in Table 3.

Also presented within Fig. 3 is the exposure limit as a function of the ratio of 860 nm content in the exposure. The exposure limit is computed based upon the assumption that the sum of the ratios of exposure to exposure-limit at the two wavelengths must sum to a value of less than one. The graph illustrates a value of 10 times the exposure limit for purposes of comparison. The trend in exposure limit provides a very good agreement with the trend predicted and measured by experiment. Most importantly, the model demonstrates that the damage threshold trend is in good agreement with the trends in the experimental data and produces a non-linear trend as a function of percentage of 860-nm content. This sub-linear behavior reflects the weighting of the damage threshold towards the 532-nm wavelength, primarily due to the much larger absorption coefficient within the retinal pigment epithelium.

The results also show that the application of the ANSI Z136.1-2000 safety standard (Lyons 1985; ANSI 2000) exposure limits provides a reasonable trend agreement for combined wavelength ratios. The exposure limit maintains a factor of greater than 10 in the ratio of damage threshold to exposure limit. At no intermediate value was there observed a synergistic effect that reduces

Table 3. Minimum visible lesion thresholds in milliwatts (fiducial limits determined at the 95% confidence interval are presented as values in parentheses).

Experimental setup Number of subjects and shots	MVL-ED_{50} 1-h reading	MVL-ED_{50} 24-h reading	Slope $\delta p/\delta d$
Eye with 532/860 = 7/1 3 subjects, 3 eyes, 70 exposures	8.4 (6.8–10.6) mW	5.6 (4.2–7.1) mW	4.0
Eye with 532/860 = 1/1 3 subjects, 3 eyes, 70 exposures	9.2 (6.4–13.1) mW	7.9 (6.1–10.0) mW	3.9
Eye with 532/860 = 1/3 2 subjects, 2 eyes, 50 exposures	10.8 (8.1–15.1) mW	9.5 (8.5–16.5) mW	21.3
Eye with 532/860 = 0/1 2 subjects, 4 eyes, 100 exposures	27.0 (21.6–39.7) mW	17.0 (14.5–20.1) mW	4.8

Table 4. Thermal model damage threshold computation results.

Power ratio (532 nm/860 nm)	Percentage 860 nm (%)	Damage threshold dosage at cornea (mW)
1/0	0	8.00
7/1	12.5	8.41
3/1	25	9.32
2/1	33.3	9.99
1/1	50	11.42
1/2	66.7	13.76
1/3	75	15.56
1/7	87.5	18.90
0/1	100	24.12

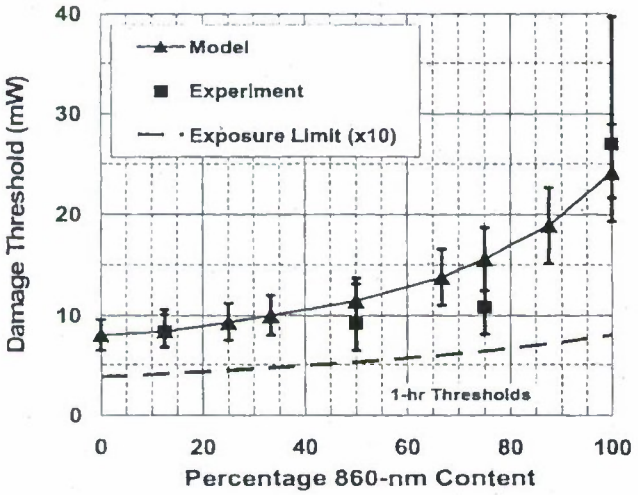

Fig. 3. Summary of 1-h damage threshold values measured, damage thresholds predicted by thermal modeling, and the current combined-wavelength exposure limit values.

the safety margin provided by the safety standard relative to the single wavelength values.

DISCUSSION

These MVL thresholds studies may be compared to previously reported values for other exposure times, wavelengths, and retinal image sizes. Table 5 lists those researchers reporting comparable measurements in live eyes showing the year of publication, wavelength, and other data relevant to our measurements. It is interesting to note that no threshold values have been reported for exposure time greater than 1 μs up to 10 s for a wavelength of 532 nm. This is due in part to the fact that there were no CW lasers producing 532 nm (doubled Nd:YAG or Nd:YVO_4) until the past few years because this wavelength could only be produced by doubling a Q-switched laser. The closest wavelength reported to the 532 nm CW is the 514 nm from the argon laser. At a wavelength of 514 nm, there were three different exposures reported between 1 to 10 s. The MVL-ED_{50} in Table 5 varied between 4.2 mW for a "small" spot size as reported by the author and 11.6 mW for the larger retinal image spot size of 500 μm. The ANSI Z136.1-2000 standard (ANSI 2000) states, "Viewing a laser from within a collimated beam produces a small (20–30 μm) or nearly diffraction limited retinal image, which will be a *small source*." It goes on to state that small source MPEs in the wavelength range of 0.4 μm to 0.6 μm are based on both thermal and photochemical effects to the retina. Both lasers that were used in this study produced small-source retinal image sizes.

The data obtained in this work for a ratio of 7/1, 532/860 nm seen in Table 3 is most comparable with data obtained from the literature shown in Table 5. We have compiled several references that contain single-wavelength exposures, at both 532 nm and 514 nm for a point of reference, as our results did not include a single-wavelength 532-nm exposure (Lappin 1970; Gallagher and Laudeieri 1973; Lund et al. 1976; Gibbons and Allen 1977; Ham et al. 1979, 1984; Onda and Kameda 1980). The measured ED_{50} was 5.6 mW for the ratioed powers of 7/1 for 10-s exposure. Other comparable data sets reported were for the 632-nm wavelength for 7.5- and 10-s exposure durations. Threshold values shown in Table 5 are 6.4 mW and 16 mW for the small and large retinal spot sizes, respectively. The driver for the comparison of these values is due to the reports that "... there is no wavelength dependence on the retinal injury thresholds between the red and green wavelengths" (Sanders and Hemstreet 1974a, b).

Table 5. MVL thresholds reported in the literature.

Author	Wavelength (nm)	Exposure time (s)	Image size	ED_{50} (mW)	Observation time (h)
Gibbons and Allen (1977)	514	5	small	5.6	24
Ham et al. (1979)	514	16	500 μm	11.6	24
Onda and Kameda (1980)	514	1	small	4.2	24
Lappin et al. (1970)	632	7.5	small	6.4	1
Ham et al. (1979)	632	16	500 μm	16	24
Gallagher and Laudeieri (1973)	860	5	476 μm	27.6	1
Lund et al. (1976)	860	8	small	19.4	1
Ham et al. (1984)	860	10	500 μm	44.3	24

For the other wavelength (860 nm), three exposure times (5–10 s) have been reported as shown in Table 5. These thresholds varied between 19.4 and 44 mW, depending on the retinal image size. The study utilizing the smallest image comparable to our retinal spot size reports a threshold of 19.4 mW at 8 s. This value compares favorably to our threshold at 10 s of 17 mW. In fact, when we plot our data point on those reported by Lund et al. (1976) we find that our results appear to follow the trend as reported and shown for clarity in Fig. 4. This figure shows how the MVL thresholds vary as a function of exposure times from 0.125 s to 10 s. Error bars in this figure represent the approximate 95% confidence interval from probit analysis procedures. In the case of Lund et al. (1976), these were approximated from figures that appear in the report but could not be determined precisely. In addition, we note relative threshold values from 532 nm to 860 nm increase by a factor of three, consistent with studies of action spectra (Lund and Edsall 1998) and powers for photocoagulation (Vogel and Birngruber 1992) found in the literature.

In Fig. 5 we compare the published exposure limits (Lyons 1985; ANSI 2000) for combined wavelengths of 532 and 860 nm vs. the ratio of powers delivered from 532 to 860 nm; that is, powers changing from a ratio of 7/1 to 0/1, respectively. This chart shows that the data for the MVL-ED_{50}s are always greater than the MPE by a factor of more than 12 for all percentages of irradiances delivered for the ratios of 532 to 860 nm used.

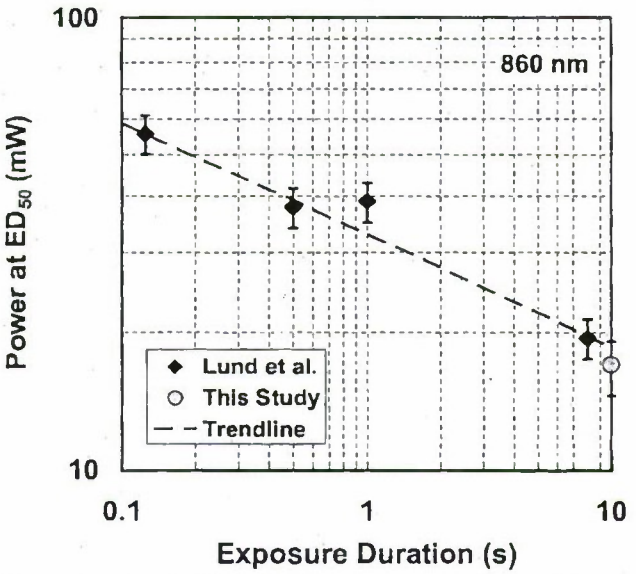

Fig. 4. MVL thresholds by Lund (Ham et al. 1984) and data from Table 1 at 860 nm. Error bars represent 95% confidence intervals in each study (the dashed trend line is a representation of time to the one-quarter power roughly fit to the data).

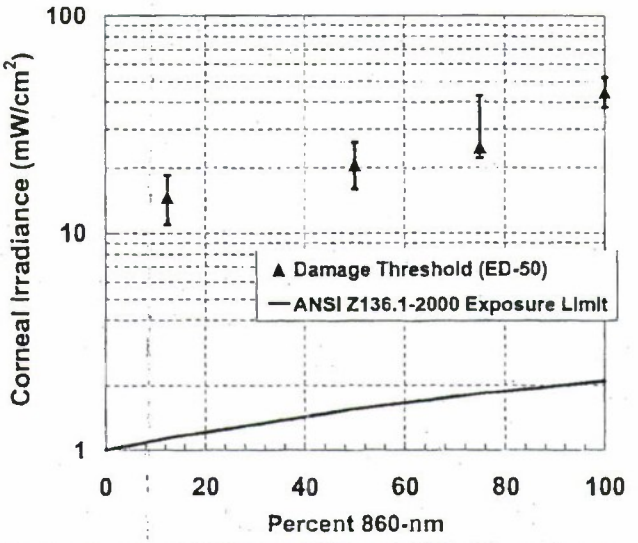

Fig. 5. Combined 532/860-nm MPEs and MVL-ED_{50}s (24 h post exposure) as percent of 860 nm.

When considering exposure time during the threshold damage measurements, shorter exposure times require higher powers to produce visible lesions. Even though we used a 10-s exposure time for all our measurements, and this is the worst-case condition, shorter exposure times may be received. In this case, as shown in Fig. 4, the power required for the MVL-ED_{50} does increase as the pulse or exposure time decreases.

CONCLUSION

From the measurements reported in this work, coupled with the ANSI-Z136 standard, there appears to be the required safety margin between the MVL thresholds and the MPEs. This is born out by independent research reported in the literature. Based on the probit analysis of our measurements for the ED_{50}, the $ED_{0.1}$ (0.001 probability) dose was calculated to be twice the ANSI-MPE for a 10-s exposure for the combined wavelengths of 532 and 860 nm in a power ratio of 7/1. Thus, at twice the ANSI-MPE value, there is a small but finite possibility that a visible lesion could occur from exposure to simultaneous wavelengths from a laser system. Further, it has been shown here that there is at least a factor of 12 difference between the MPE and the MVL-ED_{50} in live rhesus eyes, and this value increases as the percentage of 860 nm increases to 100%. Thus, there is a slightly greater safety margin for 860 nm when compared with the 532-nm wavelength. No evidence of damage to the retina was found when live eyes were exposed for 10 s to an equivalent irradiance of that produced by the simultaneous combination of the two laser wavelengths studied. Finally, we believe that this validating data for our

retinal damage model for multi-wavelength exposures is invaluable. The capability to evaluate multiple-laser exposures to the retina in cases of differing beam sizes and absorption parameters is a new tool in evaluating the safety of a potential application.

Acknowledgments—The authors gratefully acknowledge AFOSR support from the Air Force Research Laboratory Human Effectiveness Directorate. Research performed by Northrop Grumman and Fort Hays State University was conducted under USAF Contract Number F41624-02-D-7003.

Disclaimer—In conducting the research described in this work, the investigators adhered to the "Guide for the Care and Use of Laboratory Animals," as promulgated by the Committee on Revision of the Guide for Laboratory Animal Facilities and Care, Institute of Laboratory Animal Resources, National Academy of Sciences-National Research Council. The opinions or assertions contained herein are the private views of the authors and are not the official recommendations, and do not reflect the views of Fort Hays State University, the Department of the Air Force, or the Department of Defense.

REFERENCES

American National Standards Institute. American National Standard for safe use of lasers. Washington, DC: ANSI; ANSI-Z136.1; 2000.

Birngruber R, Gabel V-P, Hillenkamp F. Experimental studies of laser thermal retinal injury. Health Phys 44:519–531; 1983.

Birngruber R, Hillenkamp F, Gabel VP. Theoretical investigations of laser thermal retinal injury. Health Phys 48:781–796; 1985.

Boettner EA. Spectral transmission of the eye. Ann Arbor, MI: The University of Michigan; AF41(609)-2966; 1967.

Cain CP, Noojin GD. A comparison of various probit methods for analyzing yes/no data on a log scale. Brooks AFB, TX: USAF Armstrong Laboratory; AL/OE-TR-1996-0102; 1996.

Finney DJ. Probit analysis. New York: Cambridge University Press; 1971.

Gallagher JT, Laudeieri PC. Hazard evaluation of a gallium arsenide diode array laser. Brooks AFB, TX: USAF School of Aerospace Medicine; SAM-TR-73-19; 1973.

Gibbons WD, Allen RG. Retinal damage from long-term exposure to laser radiation. Investigative Ophthalmol Visual Sci 16:521–529; 1977.

Ham WT, Mueller HA, Ruffolo JJ, Clarke AM. Sensitivity of the retina to radiation damage as a function of wavelength. Photochem Photobiol 29:735–743; 1979.

Ham WT, Mueller HA, Ruffolo JJ, Guerry RK, Clarke AM. Ocular effects of GaAs lasers and near infrared radiation. Applied Optics 23:2181–2186; 1984.

Lappin PW. Ocular damage thresholds for the helium-neon laser. Archives Environmental Health 20:177–183; 1970.

Lund DJ, Edsall PR. Action spectrum for the retinal thermal injury. In: Matthes R, Sliney DH, eds. Measurement of optical radiation hazards. Oberschleibheim: ICNIRP; 1998: 209–228.

Lund DJ, Adams DO, Carver C. Ocular hazard of the GaAs laser. Presidio of San Francisco, CA: Letterman Army Institute of Research; Final Report; 1976.

Lyons TL. Hazard analysis technique for multiple wavelength lasers. Health Phys 49:221–226; 1985.

Maher EF. Transmission and absorption coefficients for ocular media of the Rhesus monkey. Brooks Air Force Base: USAF School of Aerospace Medicine; SAM-TR-78-32; 1978.

Mainster MA, White TJ, Allen RG. Spectral dependence of retinal damage produced by intense light sources. J Optical Society America 60:848; 1970a.

Mainster MA, White TJ, Tips JH, Wilson PW. Transient thermal behavior in biological systems. Bull Math Biophys 32:303–314; 1970b.

Neumann J, Brinkmann R. Boiling nucleation on melanosomes and microbeads transiently heated by nanosecond and microsecond laser pulses. J Biomed Optics 10:1–12; 2005.

Onda Y, Kameda T. Studies of laser hazards and safety standards (Part 3: Retinal damage thresholds for argon lasers). U.S. Army Intelligence and Information Agency; USAMIIA-K-9992; 1980.

Peaceman DW, Rachford HH. The numerical solution of parabolic and elliptic differential equations. J Soc Industrial Applied Mathematics 3:28–41; 1955.

Sanders VE, Hemstreet HW. 1st Annual Report, Part I, on Contract F41609-73-C-0017. Brooks AFB, TX: USAF School of Aerospace Medicine; 1974a.

Sanders VE, Hemstreet HW. 2nd Annual Report, Part V, on Contract F41609-73-C-0017. Brooks AFB, TX: USAF School of Aerospace Medicine; 1974b.

Takata AN, Goldfinch L, Hinds JK, Kuan LP, Thomopoulis N, Weigandt A. Thermal model of laser-induced eye damage. Brooks AFB, TX: USAF School of Aerospace Medicine; IITRI J-TR-74-6324; 1974.

Takata AN, Zaneveld D, Richter MS. Laser induced thermal damage of skin. Brooks Air Force Base, TX: USAF School of Aerospace Medicine; SAM-TR-77-38; 1977.

Thomas RJ, Noojin GD, Stolarski DJ, Hall RM, Cain CP, Toth CA, Rockwell BA. Comparative study of ocular damage thresholds from continuous-wave and femtosecond mode-locked lasers. Laser and noncoherent light ocular effects. Epidemiol Prevention Treatment 4246:54–62; 2001.

Vogel A, Birngruber R. Temperature profiles in human retina and choroid during laser coagulation with different wavelengths ranging from 514 to 810 nm. Lasers Light Ophthalmol 5:9–16; 1992.

Welch AJ, Polhamus GD. Measurement and prediction of thermal injury in the retina of the rhesus monkey. IEEE Trans in Biomed Eng MVE 31:633; 1984.

Welch AJ, Van Gemert M. Thermal response of tissue to optical radiation. New York: Plenum Press; 1995.

Welch AJ, Priebe LA, Forster LD, Gilbert R, Lee C, Drake P. Experimental validation of thermal retinal models of damage from laser radiation. Austin: University of Texas; Contract F33615-76-C-0605; 1978.

■ ■